




Bulk nanocomposite made of ZnO lamellae embedded in the ZnWO₄ matrix: growth from the melt

Monika Tomczyk^{1,*} , Paweł Osewski², Marie-Helene Berger³, Ryszard Diduszko², Iwona Józwiak², Giorgio Adamo^{4,5}, and Dorota A. Pawlak^{1,2,6,*}

¹ Faculty of Chemistry, University of Warsaw, Pasteura 1, 02-093 Warsaw, Poland

² Őukasiewicz Research Network-Institute of Microelectronics and Photonics, al. Lotników 32/46, 02-668 Warsaw, Poland

³ Centre des Matériaux, CNRS UMR 7633, MINES Paristech, 10 Rue Henri Desbrières, BP 87, 91003 Evry Cedex, France

⁴ Optoelectronics Research Centre, University of Southampton, Highfield, Southampton SO17 1BJ, UK

⁵ Present address: Centre for Disruptive Photonic Technologies, The Photonics Institute, School of Physical and Mathematical Sciences, Nanyang Technological University, Singapore 637371, Singapore

⁶ ENSEMBLE3 sp. z o.o., Wolczyńska 133, 01-919 Warsaw, Poland

Received: 22 December 2020

Accepted: 16 March 2021

Published online:

1 April 2021

© The Author(s) 2021

ABSTRACT

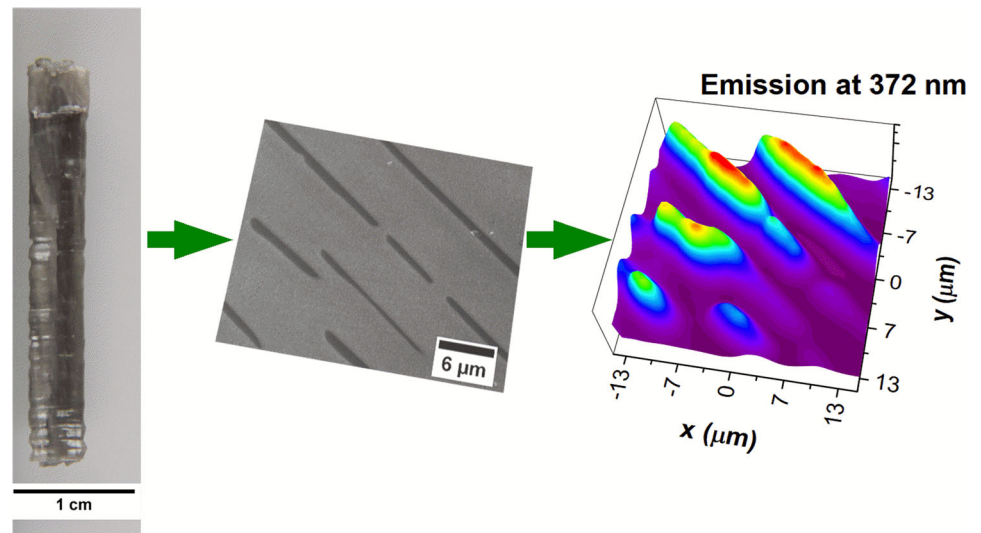
Zinc oxide (ZnO) nanostructures exhibiting high exciton binding energy and efficient radiative recombination, even at the room temperature, are of increasing interest due to their prospective exploitation in optoelectronic and laser applications. However, attempts to synthesize well-ordered structures through simple and fast process have faced many difficulties. Here, we demonstrate a novel manufacturing method of ZnO lamellae embedded in a crystalline wide band gap dielectric matrix of the zinc tungstate, ZnWO₄. The manufacturing method is based on a directional solidification of a eutectic composite, directly from the melt, resulting in a nanostructured bulk material. Electron microscopy studies revealed clear phase separation between the ZnO and ZnWO₄ phases, and cathodoluminescence confirmed exciton emission at room temperature and thus high quality and crystallinity of the ZnO lamellae, without defect emission. Hence, utilization of directional solidification of eutectics may enable cost-efficient manufacturing of bulk nanostructured ZnO composites and their use in optical devices.

Handling Editor: David Cann.

Address correspondence to E-mail: mtomczyk@chem.uw.edu.pl; Dorota.Pawlak@itme.edu.pl

<https://doi.org/10.1007/s10853-021-06020-y>

GRAPHICAL ABSTRACT



Introduction

Zinc oxide has received much attention in recent years because it exhibits a wide range of favorable properties. The lack of a center of symmetry and large electromechanical coupling give rise to strong piezoelectric and pyroelectric properties and the resulting use of ZnO in mechanical actuators and piezoelectric sensors [1]. Moreover, ZnO is a wide band gap (3.37 eV) semiconductor that is suitable for short wavelength optoelectronic applications, and its high exciton binding energy (60 meV) can ensure efficient excitonic emission at room temperature [2]. ZnO is also biocompatible, biodegradable, and bio-safe for medical and environmental application and shows good photocatalytic activity [3]. Hence, ZnO may be considered for an extensive range of applications such as energy storage, sensors, cosmetic products, optoelectronic and electronic devices, among others [4]. Recently, ZnO nanostructures have received broad attention due to their unique properties [5]. In particular, they have been widely used for sensing applications because of their high sensitivity to the chemical environment. ZnO nanowires have the advantage of a high surface area and have demonstrated high sensitivity, even at the room

temperature, whereas ZnO thin film gas sensors often need to be operated at elevated temperatures [6]. Lasing in ZnO nanowire arrays grown by a variety of methods has been observed by different research groups, and single nanowire light-emitting diode was presented as well [7]. Moreover, well-aligned single-crystalline nanowires were proposed for use as high-aspect-ratio probes for atomic force microscopy (AFM) [7]. Recently, ZnO nanostructured films have been also used in dye-sensitized solar cells as an electrode material [6].

High-quality crystals can, in principle, be grown from the melt. However, despite several trials [8], it is not really possible, since ZnO decomposes into atomic components below the melting point, 1975 °C, at atmospheric pressure [9]. However, this can be overcome with a eutectic transition, where from a one-phase melt a two-solid-phases composite material is crystallized at much lower melting temperature than its constituent phases, enabling growth of phases like the ZnO.

Directional solidification of eutectics has been considered as a promising method to fabricate bulk, highly crystalline and self-organized nano-/microstructures out of various materials combinations, with a plethora of geometrical motifs, controllable structure refinement and sharp interfaces [10].

Recently, directional solidification of eutectics was utilized for energy materials such as solid-oxide fuel cells [11, 12] and electrodes for hydrogen generation [13, 14], and optical materials such as photonic crystals [15, 16]; THz polaritonic materials [17, 18]; metamaterials [19–23] and nanoplasmonic materials [24–26]. It has been also shown that eutectic composites could exhibit unusual geometries when properly engineered [27–29], in addition to being grown as bulk materials [30] even on the industrial scale and also printed [31].

In this work, we utilize the eutectic directional solidification for manufacturing of well-ordered ZnO layers directly from the melt. The ZnO ca. 250-nm-thick layers are embedded in the ZnWO₄ matrix forming a bulk ZnO-ZnWO₄ material. The growth of the composite by the micro-pulling down method is presented. The optical response of the obtained nanostructured ZnO composites was assessed by cathodoluminescence studies.

Materials and methods

Crystal growth

ZnO-ZnWO₄ eutectic rods were grown by the micro-pulling down method using Cyberstar commercial equipment. This method utilizes a metallic crucible with a shaper at the bottom and a centrally placed nozzle (Fig. 1a). Starting charge material is placed in the crucible which is then mounted in the furnace. The raw materials are molten in the crucible; the melt exudes through the nozzle and wets the bottom of the shaper. The molten material is kept by the surface tension, liquid viscosity and cohesion forces between the liquid and the crucible. Then, the molten material is touched with the seed crystal, and the seed with the growing rod is pulled down. The growth atmosphere was nitrogen, and a SrLaGaO₄ crystal was used as a seed [32]. The growing process was controlled by adjustment of power and pulling rate. In this case, to obtain good quality with homogeneous distribution of ZnO precipitates in the whole volume of the rod, an iridium crucible (Heraeus Holding GmbH) with a rectangular die 3 × 5 mm and a slit of 1 × 3 mm was used. A picture of the crucible and its cross-sectional scheme are shown in Fig. 1b, c.

High-purity ZnO (99.9999%) and WO₃ (99.999%) oxide powders were used as starting materials. The

oxide powders were mixed with ethanol in an agate mortar and dried at 350 °C, and then, the charge material was loaded into a crucible and heated up.

The growth processes were monitored by CCD camera, and the temperature was measured using a Raytek MM2MH pyrometer. The emissivity of the iridium crucible used during the growth was determined experimentally and was equal to 0.46 for the 1.6 μm spectral range and the temperature range of 900 to 1200 °C. The measured area was 1 mm in diameter and was located on the wall of the crucible as close as possible to the growth zone. Figure 1e shows the crystallization front, growing fiber and the temperature measurement area.

The process was controlled manually by changing the pulling rate and output power of generator at the initial stage of growth in order to obtain a crystallization front as thin as possible and parallel to the surface of the shaper. After stable thermodynamic conditions of the growth were obtained, only the output power of the generator was changed to control the parameters of the crystallization front and the pulling rate was kept constant. Figure 1f shows the temperature recorded during the process. The rapid rise of temperature after 30 min of the heating procedure was related to the change in emissivity of the crucible, as molten material began to climb on the walls of the crucible during seeding process. Then, the thermodynamic conditions were stabilized and the growth started. The temperature was raised from 1170 °C to the melting point of ZnO-ZnWO₄ eutectic 1190 ± 20 °C [33]. The increase in temperature around the 7th hour was due to re-climbing of molten material on the wall of crucible. However, it did not affect the growth of the eutectic rod and its quality. After a period of stable growth, the temperature was increased to detach the eutectic fiber from the bottom of the crucible, and cooling was started. The as-grown ZnO-ZnWO₄ eutectic rod is presented in Fig. 1g.

Phase and micro/nanostructure characterization

The crystallographic structure and phase content of the ZnO-ZnWO₄ eutectic were analyzed by powder X-ray diffraction (XRD) using a Siemens D500 diffractometer equipped with a semiconductor Si/Li detector and K_αCu radiation. The diffraction patterns were measured in $\theta/2\theta$ scanning mode with a step of

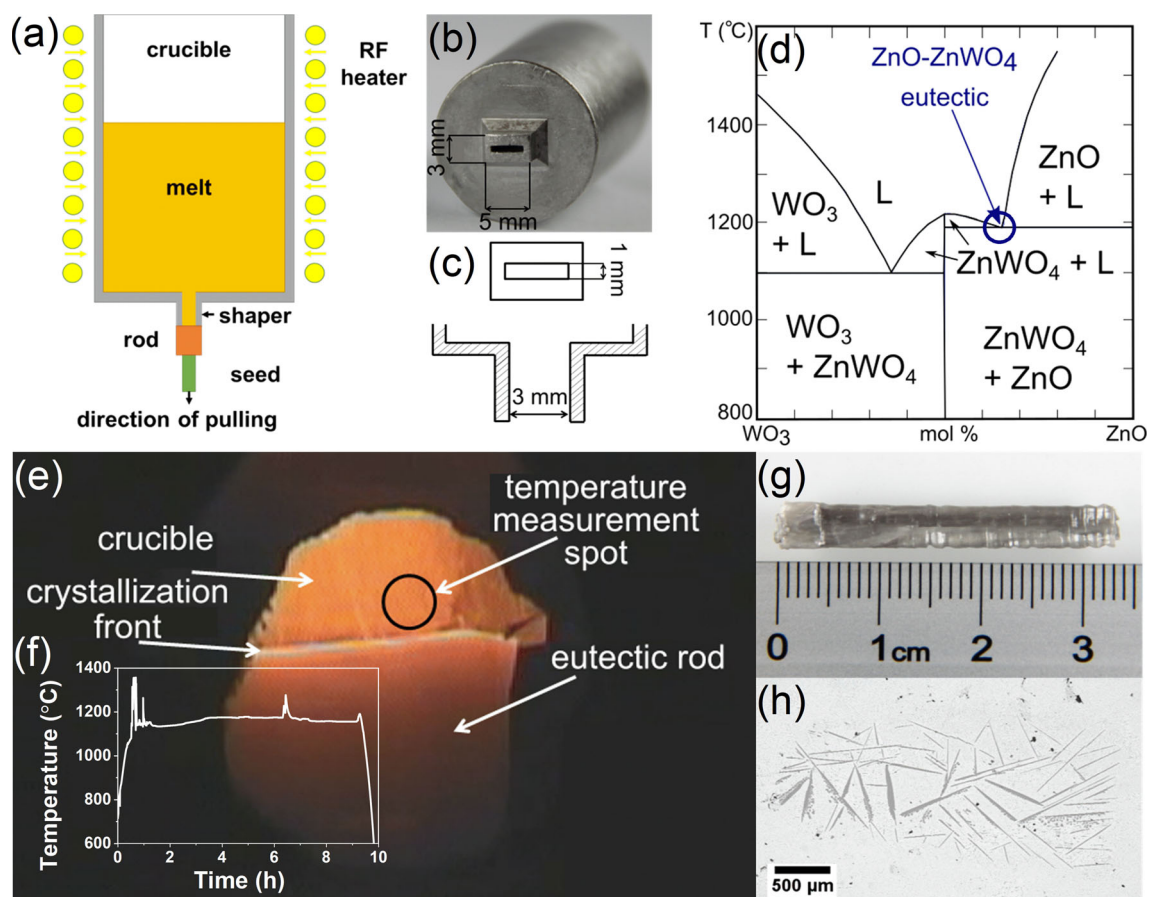


Figure 1 ZnO–ZnWO₄ eutectic composite grown from the melt by the micro-pulling-down method. **a** μ -PD method thermal set-up scheme. **b** Image of the crucible and **c** scheme of used crucible shaper and nozzle. **d** Phase diagram of the ZnO–WO₃ eutectic system. **e** Image of the crucible shaper, growing eutectic rod, crystallization front and place where the temperature was measured

with the pyrometer. **f** Temperature pattern of crucible around the crystallization front. **g** The as-grown eutectic rod. **h** The scanning electron microscope image of the big ZnO precipitates inside the central area—a core effect observed in non-optimized growth conditions.

0.02° and counting time of 10 s/step. The experimental data were analyzed by Rietveld refinement using the R. A. Young DBWS-9807 program package. Microstructure characterization was carried out with scanning electron microscope (SEM) Auriga® CrossBeam® Workstation (Carl Zeiss) equipped with an energy-dispersive spectroscopy detector (EDS) for chemical composition analysis.

This dual beam workstation was also used for focused ion beam SEM (FIB-SEM) tomography. Serial FIB cross sections in situ milling was performed by Ga-ion beam. For each slice, SEM images (image size 1024 × 768 pixels, 24 bit grayscale) were taken. The crystal orientation relationship between the two phases and interface planes were determined using a transmission electron microscope (TEM) FEI Tecnai F20ST, FEG 200 keV.

Cathodoluminescence

Cathodoluminescence (CL) measurements were taken with SEM (CamScan CS3200 with a LaB6 cathode) at the Centre of Optoelectronics, the University of Southampton. The electron beam was focused onto the sample via a parabolic mirror mounted directly above it. The mirror collected the light emitted from the sample and directed it out of the SEM chamber to a Horiba spectrometer with a liquid-nitrogen-cooled CCD detector. The covered spectral range was 250–1000 nm using 1024 channels. During the CL spectra measurement, beam current of probe varied between areas of interest; therefore, recorded spectra were normalized.

Results and discussion

In order to demonstrate the possibility of utilizing directional solidification of eutectics for manufacturing ZnO nanostructured materials in a bulk form directly from the melt, we have grown rods with the eutectic composition of 65 mol % ZnO and 35 mol % of WO_3 , marked on the WO_3 -ZnO phase diagram in Fig. 1d [33]. According to Shchenev et al., the ZnO- WO_3 equilibrium phase diagram encloses only one ternary compound ZnWO_4 and two eutectic invariant points [33]. The ZnO- ZnWO_4 eutectic at 65 mol% of ZnO and 35 mol% of WO_3 molar ratio allows the solidification of ZnO as one of the component phases. The melting temperature at the eutectic point is about 1187 °C, which is much lower than the melting point of ZnO (1975 °C) [4] and WO_3 (1473 °C) [33]. The melting point is low enough to allow the coexistence of solid and liquid phases of ZnO and, under these conditions, the material does not decompose. Eutectic rods were obtained with a pulling rate of 0.1 and 0.5 mm/min. At the initial stage of growth, when the thermodynamic conditions were not stable, large ZnO inclusions ($400 \times 40 \mu\text{m}$) could be observed within the eutectic rod core as shown in the SEM image (Fig. 1h). After stabilization of eutectic growth conditions, large inclusions of ZnO were not observed.

The XRD demonstrated two phases in the obtained rods, Fig. 2a. The diffraction peaks match well the standard diffraction pattern of wurtzite ZnO phase (JCPDS-04-015-4060) and wolframite ZnWO_4 phase (JCPDS-04-009-8448) with no evidence of any extra phase within the XRD detection limits. The lattice parameters deduced by Rietveld refinement of the XRD profile of ZnO- ZnWO_4 eutectic are $a = 3.25 \text{ \AA}$ and $c = 5.21 \text{ \AA}$ for ZnO and $a = 4.69 \text{ \AA}$, $b = 5.72 \text{ \AA}$, $c = 4.93 \text{ \AA}$, $\beta = 90.64^\circ$ for ZnWO_4 and match well the previously reported values [34, 35]. The plane orthogonal to the growth direction was determined from bulk crystal samples. They correspond to $(10\bar{1}0)$ ($2\theta = 32^\circ$) and $(11\bar{2}0)$ ($2\theta = 56^\circ$) for the ZnO and (001) ($2\theta \sim 36^\circ$ and $2\theta \sim 72^\circ$) and (013) ($2\theta \sim 57^\circ$) for ZnWO_4 , the last one giving rise to a weaker diffraction signal.

The SEM images and EDS studies Fig. 2b, c revealed a eutectic micro/nanostructure consisting of ZnO lamellae/layers embedded in the ZnWO_4 matrix in the entire volume of the eutectic rods regardless of

the thermodynamic conditions of growth, Fig. 3a–c. In the whole volume of sample, eutectic grains as big as $100 \times 100 \mu\text{m}^2$ and more were observed. Within one grain, ZnO lamellae were parallel to each other and their thickness was approx. 250 nm.

In order to reconstruct the microstructure of ZnO- ZnWO_4 eutectic in three dimensions (3D), the FIB-SEM technique was used. In this technique, the sample is sequentially milled using an ion beam perpendicular to the specimen while imaging the newly exposed surface using an electron beam. A thorough analysis of sectional micrographs perpendicular to the growth axis recorded using FIB-SEM technique confirms that the ZnO- ZnWO_4 eutectic crystallizes in the broken-lamellar structure, Fig. 3d [36]. The characteristic feature of the eutectic with broken-lamellar structure is the small volume ratio of the lamellar phase to the matrix phase. The minor ZnO phase appears as broken lamellae in the 2D microstructure, but FIB-SEM shows that the ZnO phase is continuous and occurs as perforated plates with holes filled with ZnWO_4 matrix phase. This broken lamellar type microstructure obviously represents a structure dictated by a long-range force favoring lamellar morphologies. However, a short-range force (instability perhaps) clearly exists which “breaks” the lamellae [37]. As suggested by Beghi, the relatively large interlamellar spacings and thin lamellae observed in low-volume-fraction eutectics require large diffusion distances. Therefore, it seems quite possible that thermally induced local irregularities in the solute concentration or diffusional flow in the melt could produce the irregular “breaks” as seen in two dimensions or “holes” in three dimensions [38].

The ZnO- ZnWO_4 eutectics have been further studied using high-resolution TEM (HRTEM). The thin foil was extracted from a plane containing the growth axis. In order to study the crystal orientation relationship between the ZnO and ZnWO_4 and to define the interface planes, diffraction studies were performed (Fig. 4). Figure 4a shows a selected area electron diffraction (SAED) pattern of the ZnWO_4 . When the thin foil is perpendicular to the electron beam, no simple zone axis can be obtained for the matrix. Only the $[001]^*$ reciprocal direction can be imaged, indicating that the (001) plane of the ZnWO_4 matrix is perpendicular to the surface of the FIB foil. With a few degrees tilt, the foil is oriented in $[100]$ zone axis, Fig. 4a with the 001 reflection obtained by

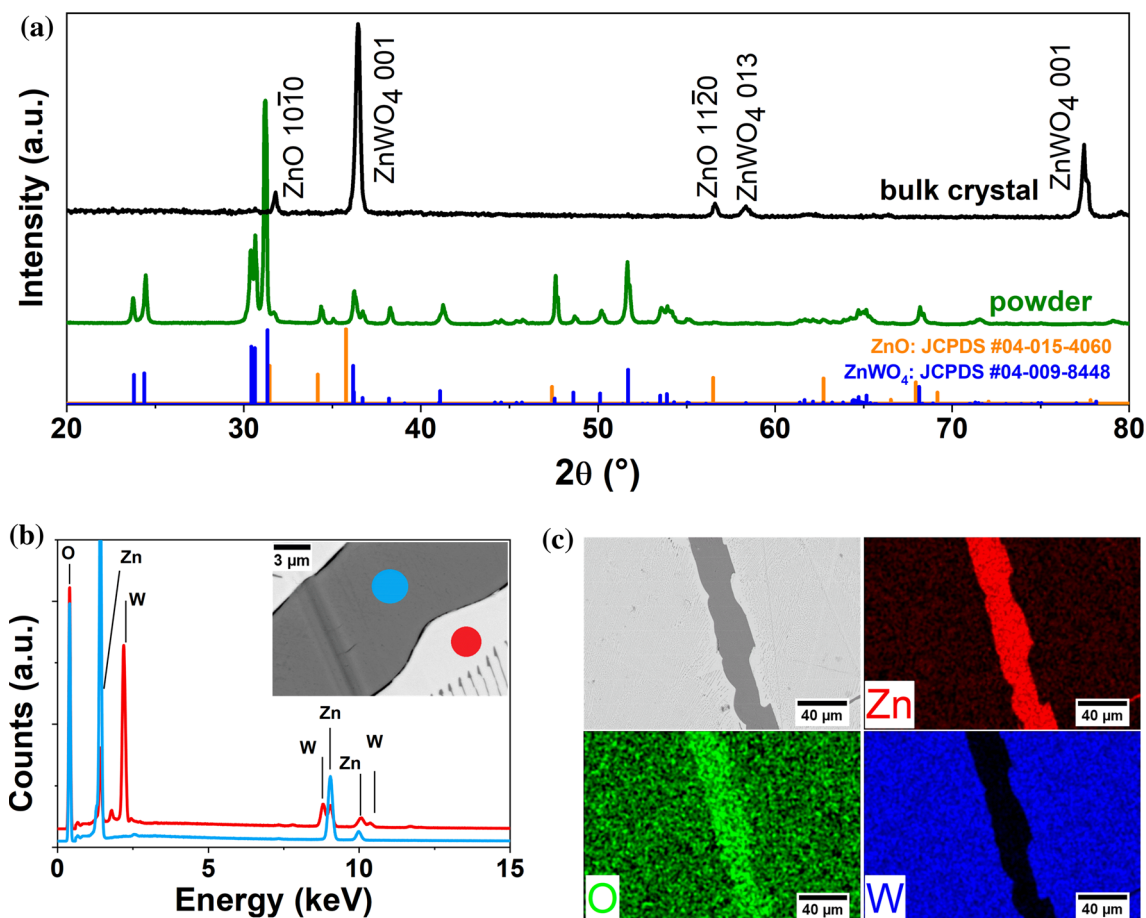


Figure 2 Phase and chemical analysis of the obtained ZnO–ZnWO₄ eutectic composite. **a** X-ray diffraction revealing two phases: ZnO and ZnWO₄ and two different growth orientations for

double diffraction (dd). For the same tilt angles, the ZnO lamella does not show a simple zone axis but the [0001]* reciprocal direction for ZnO (Fig. 4b). Figure 4c depicts diffraction patterns recorded at the interface, to superpose the two patterns. The (0002) planes of ZnO are parallel to the (020) planes of ZnWO₄ as their inter-planar distances are compatible (d_{020} . ~ 0.286 nm for ZnWO₄ and d_{0002} . ~ 0.260 nm for ZnO). The HRTEM image of the interface between (010) ZnWO₄ and (0002) ZnO is shown in Fig. 4d. Based on the TEM observation, the orientation relationship for the ZnO lamellae and ZnWO₄ matrix is defined as $[1\bar{1}00]$ ZnO almost // $[100]$ ZnWO₄ (less than 5° mismatch) and planes (0001) ZnO // (010) ZnWO₄.

Figure 5a shows the CL spectra acquired for ZnO–ZnWO₄. The spectra consist of two emission peaks at about ~ 371 and ~ 498 nm. The peak at 371 nm (UV luminescence) is attributed to near band edge

both phases. **b** Energy-dispersive spectra (EDS) and **c** maps of both phases showing that the ZnO phase forms the precipitates and the matrix is the ZnWO₄ phase.

(NBE) emission [39], which originates from the recombination of free-excitons through an exciton–exciton collision process in ZnO. The other peak ~ 498 nm is usually attributed by intrinsic tungstate emission. The WO₆ octahedra and a slight deviation from perfect order in the crystal structure are responsible for blue light emission band of ZnWO₄ [40]. Only UV luminescence (~ 373 nm) was observed for ZnO lamellae, whereas the ZnWO₄ matrix exhibited a broad band emission centered at 498 nm. The study of luminescence properties of ZnO–ZnWO₄ eutectic component phases independently reveals that the blue/green luminescence originates only from the ZnWO₄ phase. No green and blue luminescence has been detected in ZnO. In contrast to our ZnO–ZnWO₄ eutectic composite, the photoluminescence (PL) studies on (ZnO)_{1-x}(ZnWO₄)_x ($x = 0, 0.1, 0.2, 0.3, 0.5, 0.7, 0.9, 1$) nanocomposite prepared by precipitation method revealed

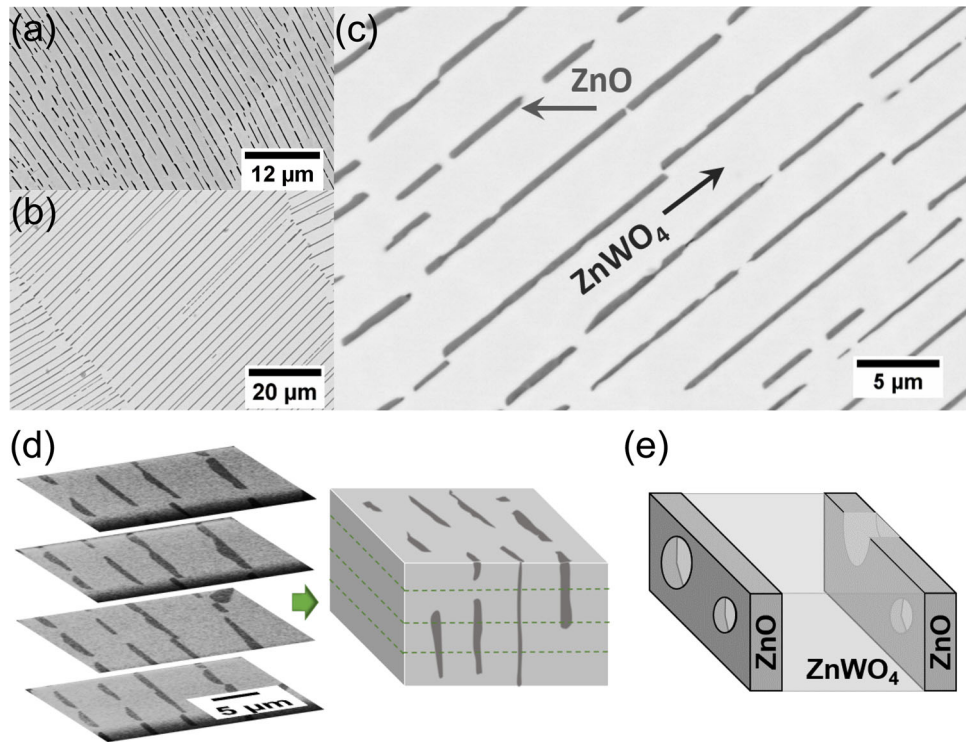


Figure 3 Broken-lamellar micro-/nanostructure of the ZnO–ZnWO₄ eutectic composite. **a** SEM image for the eutectic rod grown with the pulling rate p.r. = 0.5 mm/min, **b** eutectic grains (p.r. = 0.1 mm/min). **c** High-magnification image of the eutectic micro-/nanostructure observed in stable thermodynamic conditions, outside the core zone; ZnO layers (av. ~ 240 nm

thick) embedded in the ZnWO₄ matrix (p.r. = 0.1 mm/min). **d** FIB-SEM images of the sections perpendicular to the growth axis and reconstructed 3D model confirming the broken-lamellar character of the micro/nanostructure. **e** A scheme of the broken-lamellar structure.

Figure 4 Crystal orientation relationship between the ZnO and ZnWO₄ phases as investigated by transmission electron microscopy. Selected area diffraction pattern of **a** the ZnWO₄ matrix, **b** the ZnO lamella, and **c** the eutectic composite. **d** HRTEM image of the (010)_{ZnWO₄}//(0002)_{ZnO} interface region.

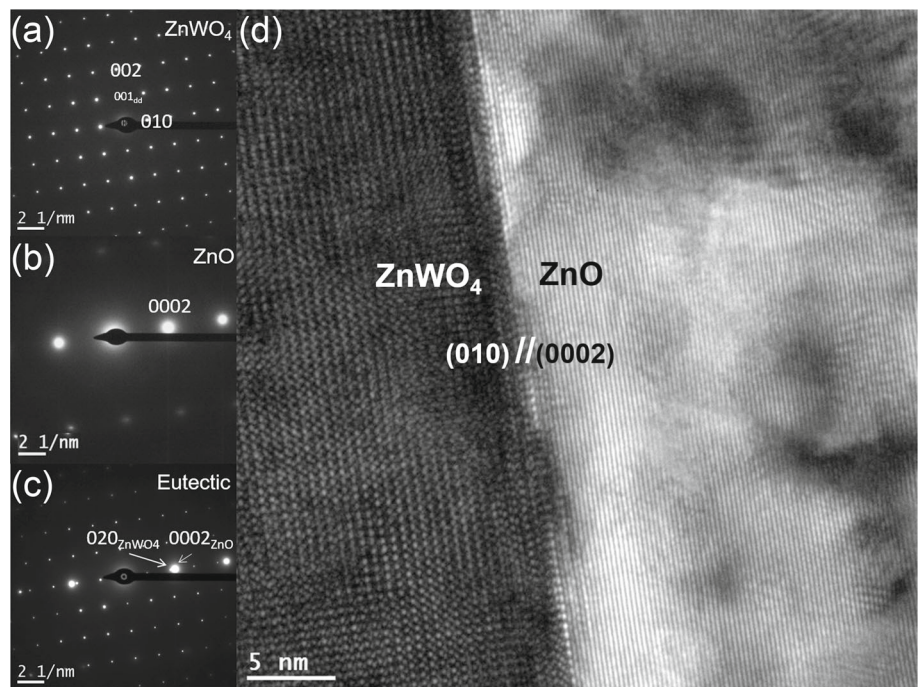
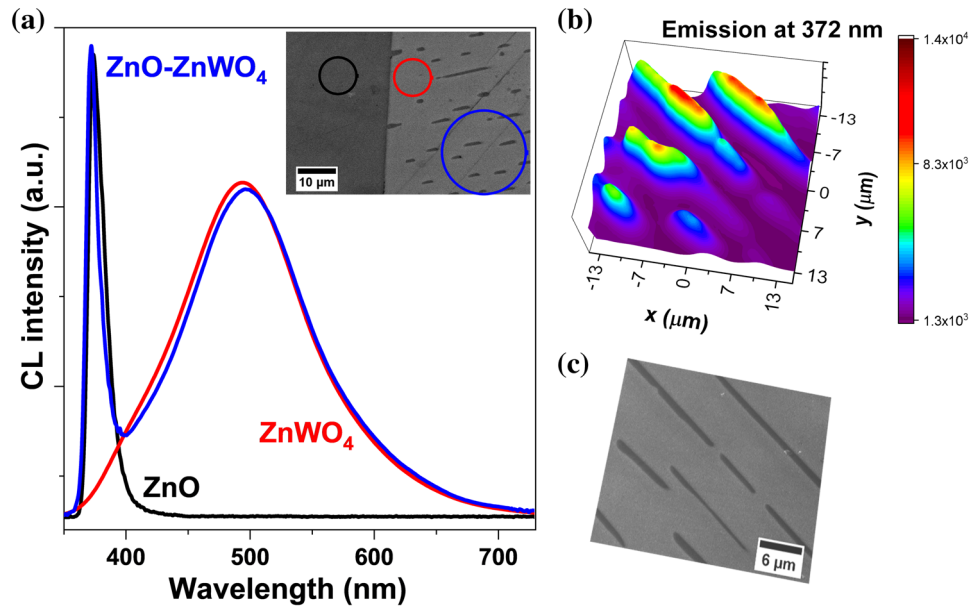


Figure 5 CL of the ZnO–ZnWO₄ eutectic. **a** CL spectra of the ZnO–ZnWO₄ eutectic and its phases. **b** CL map for ZnO NBE emission at 371 nm. **c** SEM image of the studied area.



mainly broad blue-green emission band in the range of 440–550 nm and the PL intensity of ZnO was insignificant compared with that of ZnWO₄ [41]. Figure 5b, c shows CL intensity and SEM images taken at 371 nm which corresponds to NBE emission in ZnO. The strong excitonic emission, with negligible emission in the visible range in ZnO lamellae, indicates the good optical quality of these nanostructures. Although the actual recombination mechanisms for visible emission in ZnO are still not fully understood, the absence of the visible defect-related deep level (DL) emission reveals a lower density of such defects in ZnO lamellae within the obtained eutectic composite [42].

Conclusions

A new eutectic with 65 mol% ZnO and 35 mol% WO₃ composition has been grown, and its structural and optical properties have been studied. The presence of only two phases, ZnO and ZnWO₄, has been confirmed by XRD and SEM. The ZnO–ZnWO₄ eutectic tends to grow with a broken-lamellar structure, with the ZnO phase forming perforated nanolamellae embedded in the ZnWO₄ matrix. Growth of ZnO–ZnWO₄ eutectic is an excellent platform for achieving ZnO nanostructures with high crystal quality and low density of defects as assessed by

cathodoluminescence. Such a bulk yet nanostructured ZnO material exhibiting ZnO lamellae/layers could work as optoelectronic elements which can be cut from the volumetric material and polished. Potential applications could include filters [43], polaritonic lasers [44], efficient second harmonic generators [45], ultraviolet photodetectors and optical switches [46].

Acknowledgements

The authors thank the TEAM/2016-3/29 Grant within the TEAM program of the Foundation for Polish Science co-financed by the European Union under the European Regional Development Fund and the HARMONIA Project (2013/10/M/ST5/00650) from the National Science Centre.

Author's contribution

The manuscript was written through contributions of all authors. All authors have given approval to the final version of the manuscript.

Declarations

Conflict of interest The authors declare that they have no conflict of interest.

Open Access This article is licensed under a Creative Commons Attribution 4.0 International License, which permits use, sharing, adaptation, distribution and reproduction in any medium or format, as long as you give appropriate credit to the original author(s) and the source, provide a link to the Creative Commons licence, and indicate if changes were made. The images or other third party material in this article are included in the article's Creative Commons licence, unless indicated otherwise in a credit line to the material. If material is not included in the article's Creative Commons licence and your intended use is not permitted by statutory regulation or exceeds the permitted use, you will need to obtain permission directly from the copyright holder. To view a copy of this licence, visit <http://creativecommons.org/licenses/by/4.0/>.

References

- [1] Wang X, Song J, Wang ZL (2007) Nanowire and nanobelt arrays of zinc oxide from synthesis to properties and to novel devices. *J Mater Chem* 17:711. <https://doi.org/10.1039/b616963p>
- [2] Janotti A, Van de Walle CG (2009) Fundamentals of zinc oxide as a semiconductor. *Rep Prog Phys* 72:126501. <https://doi.org/10.1088/0034-4885/72/12/126501>
- [3] Zhang Y, Ram MK, Stefanakos EK, Goswami DY (2012) Synthesis, characterization, and applications of ZnO nanowires. *J Nanomater* 2012:1–22. <https://doi.org/10.1155/2012/624520>
- [4] Özgür Ü, Hofstetter D, Morkoç H (2010) ZnO devices and applications: a review of current status and future prospects. *Proc IEEE* 98:1255–1268. <https://doi.org/10.1109/JPROC.2010.2044550>
- [5] Wang ZL (2004) Zinc oxide nanostructures: growth, properties and applications. *J Phys Condens Matter* 16:R829–R858. <https://doi.org/10.1088/0953-8984/16/25/R01>
- [6] Djurišić AB, Chen X, Leung YH, Man Ching Ng A (2012) ZnO nanostructures: growth, properties and applications. *J Mater Chem* 22:6526. <https://doi.org/10.1039/c2jm15548f>
- [7] Schmidt-Mende L, MacManus-Driscoll JL (2007) ZnO nanostructures, defects, and devices. *Mater Today* 10:40–48. [https://doi.org/10.1016/S1369-7021\(07\)70078-0](https://doi.org/10.1016/S1369-7021(07)70078-0)
- [8] Jacobs K, Schulz D, Klimm D, Ganschow S (2010) Melt growth of ZnO bulk crystals in Ir crucibles. *Solid State Sci* 12:307–310. <https://doi.org/10.1016/j.solidstatesciences.2009.05.015>
- [9] Morkoç H, Özgür U (2009) Zinc oxide: fundamentals, materials and device technology. Wiley-VCH
- [10] Lorca J, Orera VM (2006) Directionally solidified eutectic ceramic oxides. *Prog Mater Sci* 51:711–809. <https://doi.org/10.1016/J.PMATSCI.2005.10.002>
- [11] Laguna-Bercero MA, Larrea A, Merino RI et al (2005) Stability of channeled Ni-YSZ cermets produced from self-assembled NiO-YSZ directionally solidified eutectics. *J Am Ceram Soc* 88:3215–3217. <https://doi.org/10.1111/j.1551-2916.2005.00540.x>
- [12] Cubero A, Peña JI, Laguna-Bercero MA (2015) Optimization of Ni-YSZ solid oxide fuel cell anodes by surface laser melting. *Appl Surf Sci* 335:39–43. <https://doi.org/10.1016/j.apsusc.2015.01.230>
- [13] Wysmulek K, Sar J, Osewski P et al (2017) A SrTiO₃-TiO₂ eutectic composite as a stable photoanode material for photoelectrochemical hydrogen production. *Appl Catal B Environ* 206:538–546. <https://doi.org/10.1016/j.apcatb.2017.01.054>
- [14] Kolodziejak K, Sar J, Wysmulek K et al (2017) When eutectic composites meet photoelectrochemistry—highly stable and efficient UV–visible hybrid photoanodes. *J Catal* 352:93–101. <https://doi.org/10.1016/j.jcat.2017.04.019>
- [15] Kim J, Aagesen LK, Choi JH et al (2015) Template-directed directionally solidified 3D mesostructured AgCl–KCl eutectic photonic crystals. *Adv Mater* 27:4551–4559. <https://doi.org/10.1002/adma.201502265>
- [16] Pawlak DA, Lerondel G, Dmytruk I et al (2002) Second order self-organized pattern of terbium–scandium–aluminum garnet and terbium–scandium perovskite eutectic. *J Appl Phys* 91:9731. <https://doi.org/10.1063/1.1479752>
- [17] Merino RI, Acosta MF, Orera VM (2014) New polaritonic materials in the THz range made of directionally solidified halide eutectics. *J Eur Ceram Soc* 34:2061–2069. <https://doi.org/10.1016/J.JEURCERAMSOC.2013.10.025>
- [18] Reyes-Coronado A, Acosta MF, Merino RI et al (2012) Self-organization approach for THz polaritonic metamaterials. *Opt Express* 20:14663. <https://doi.org/10.1364/OE.20.014663>
- [19] Pawlak DA, Kolodziejak K, Turczynski S et al (2006) Self-organized, rodlike, micrometer-scale microstructure of Tb₃Sc₂Al₃O₁₂-TbScO₃: Pr eutectic. *Chem Mater* 18:2450–2457. <https://doi.org/10.1021/cm060136h>
- [20] Pawlak DA, Turczynski S, Gajc M et al (2010) How far are we from making metamaterials by self-organization? The microstructure of highly anisotropic particles with an SRR-like geometry. *Adv Funct Mater* 20:1116–1124. <https://doi.org/10.1002/adfm.200901875>
- [21] Myroshnychenko V, Stefanski A, Manjavacas A et al (2012) Interacting plasmon and phonon polaritons in aligned nano-

- and microwires. *Opt Express* 20:10879. <https://doi.org/10.1364/OE.20.010879>
- [22] Massaouti M, Basharin AA, Kafesaki M et al (2013) Eutectic epsilon-near-zero metamaterial terahertz waveguides. *Opt Lett* 38:1140. <https://doi.org/10.1364/OL.38.001140>
- [23] Acosta MF, Rodrigo SG, Martín-Moreno L et al (2017) Bioimaging: micropillar templates for dielectric filled metal arrays and flexible metamaterials (advanced optical materials 3/2017). *Adv Opt Mater*. <https://doi.org/10.1002/adom.201770017>
- [24] Sadecka K, Toudert J, Surma HB, Pawlak DA (2015) Temperature and atmosphere tunability of the nanoplasmonic resonance of a volumetric eutectic-based Bi₂O₃-Ag metamaterial. *Opt Express* 23:19098. <https://doi.org/10.1364/OE.23.019098>
- [25] Sadecka K, Gajc M, Orlinski K et al (2015) When eutectics meet plasmonics: nanoplasmonic, volumetric, self-organized, silver-based eutectic. *Adv Opt Mater* 3:381–389. <https://doi.org/10.1002/adom.201400425>
- [26] Deska R, Sadecka K, Olesiak-Bańska J et al (2017) Non-linear plasmonics in eutectic composites: second harmonic generation and two-photon luminescence in a volumetric Bi₂O₃-Ag metamaterial. *Appl Phys Lett* 110:031102. <https://doi.org/10.1063/1.4974208>
- [27] Akamatsu S, Bottin-Rousseau S, Şereföğlü M, Faivre G (2012) Lamellar eutectic growth with anisotropic interphase boundaries: experimental study using the rotating directional solidification method. *Acta Mater* 60:3206–3214. <https://doi.org/10.1016/j.actamat.2012.02.033>
- [28] Kulkarni AA, Hanson E, Zhang R et al (2020) Archimedean lattices emerge in template-directed eutectic solidification. *Nature* 577:355–358. <https://doi.org/10.1038/s41586-019-1893-9>
- [29] Tang J, Lambie S, Meftahi N et al (2021) Unique surface patterns emerging during solidification of liquid metal alloys. *Nat Nanotechnol*. <https://doi.org/10.1038/s41565-020-00835-7>
- [30] Bienkowski K, Turczynski S, Diduszko R et al (2011) Growth of a plate-shaped SrTiO₃-TiO₂ eutectic. *Cryst Growth Des* 11:3935–3940. <https://doi.org/10.1021/cg2005369>
- [31] Boley JW, Chaudhary K, Ober TJ et al (2017) High-operating-temperature direct ink writing of mesoscale eutectic architectures. *Adv Mater* 29:1604778. <https://doi.org/10.1002/adma.201604778>
- [32] Kołodziejek K, Turczyński S, Diduszko R et al (2006) Tb₃ScAlO₁₂-TbScO₃ eutectic self-organized microstructure for metamaterials and photonic crystals application. *Opto-Electron Rev*. <https://doi.org/10.2478/s11772-006-0027-8>
- [33] Shchenev A, Kargin Y, Skorikov M (1988) The ZnO-WO₃ system. *Russ J Inorg Chem* 33:2165–2167
- [34] Yang P, Yan H, Mao S et al (2002) Controlled growth of ZnO nanowires and their optical properties. *Adv Funct Mater* 12:323. [https://doi.org/10.1002/1616-3028\(20020517\)12:5%3c323::AID-ADFM323%3e3.0.CO;2-G](https://doi.org/10.1002/1616-3028(20020517)12:5%3c323::AID-ADFM323%3e3.0.CO;2-G)
- [35] Kalinko A, Kotlov A, Kuzmin A et al (2011) Electronic excitations in ZnWO₄ and Zn_xNi_{1-x}WO₄ (x=0.1–0.9) using VUV synchrotron radiation. *Open Phys* 9:432–437. <https://doi.org/10.2478/s11534-010-0108-7>
- [36] Fraś E (2003) *Krystalizacja metali*. WNT, Warszawa
- [37] Hunt JD, Chilton JP (1963) An investigation of lamellar-rod. Transitions in binary eutectics. *J Inst Met* 91:338–342
- [38] Beghi G, Piatti G, Street KN (1971) The structure of the unidirectionally solidified Al-AlSb binary eutectic. *J Mater Sci* 6:118–125. <https://doi.org/10.1007/BF00550341>
- [39] Huang MH, Wu Y, Feick H et al (2001) Catalytic growth of zinc oxide nanowires by vapor transport. *Adv Mater* 13:113–116. [https://doi.org/10.1002/1521-4095\(200101\)13:2%3c113::AID-ADMA113%3e3.0.CO;2-H](https://doi.org/10.1002/1521-4095(200101)13:2%3c113::AID-ADMA113%3e3.0.CO;2-H)
- [40] Li M, Wang X, Zhu Q et al (2020) Crystallization and architecture engineering of ZnWO₄ for enhanced photoluminescence. *CrystEngComm* 22:6398–6406. <https://doi.org/10.1039/D0CE00828A>
- [41] Jiang X, Zhao X, Duan L et al (2016) Enhanced photoluminescence and photocatalytic activity of ZnO-ZnWO₄ nanocomposites synthesized by a precipitation method. *Ceram Int* 42:15160–15165. <https://doi.org/10.1016/j.ceramint.2016.05.098>
- [42] Rodnyi PA, Khodyuk IV (2011) Optical and luminescence properties of zinc oxide. *Opt Spectrosc* 111:776–785. <https://doi.org/10.1134/S0030400X11120216>
- [43] Osewski P, Belardini A, Centini M et al (2020) new self-organization route to tunable narrowband optical filters and polarizers demonstrated with ZnO-ZnWO₄ eutectic composite. *Adv Opt Mater* 8:1901617. <https://doi.org/10.1002/adom.201901617>
- [44] Kang J-W, Song B, Liu W et al (2019) Room temperature polariton lasing in quantum heterostructure nanocavities. *Sci Adv* 5:9338. <https://doi.org/10.1126/sciadv.aau9338>
- [45] Chan SW, Barille R, Nunzi JM et al (2006) Second harmonic generation in zinc oxide nanorods. *Appl Phys B Lasers Opt* 84:351–355. <https://doi.org/10.1007/s00340-006-2292-0>
- [46] Kind H, Yan H, Messer B et al (2002) Nanowire ultraviolet photodetectors and optical switches. *Adv Mater* 14:158–160. [https://doi.org/10.1002/1521-4095\(20020116\)14:2%3c158::AID-ADMA158%3e3.0.CO;2-W](https://doi.org/10.1002/1521-4095(20020116)14:2%3c158::AID-ADMA158%3e3.0.CO;2-W)

Publisher's Note Springer Nature remains neutral with regard to jurisdictional claims in published maps and institutional affiliations.